Ionospheric delayed response to solar EUV radiation variations based on model simulations and satellite observations

Vaishnav, R.[1], Jacobi, Ch.[1], Schmölter, E.[2], Berdermann, J.[2], Codrescu, M.[3]

[1] *Institute for Meteorology, Universität Leipzig, Stephanstr. 3, 04103 Leipzig, Germany, E-mail: rajesh_ishwardas.vaishnav@uni-leipzig.de*
[2] *German Aerospace Center, Kalkhorstweg 53, 17235 Neustrelitz, Germany*
[3] *Space Weather Prediction Centre, National Oceanic and Atmospheric Administration, Boulder, Colorado, USA*

Summary: We investigate the ionospheric response to solar extreme ultraviolet (EUV) variations using the ionospheric total electron content (TEC) provided by the International GNSS Service (IGS) and the Coupled Thermosphere Ionosphere Plasmasphere Electrodynamics (CTIPe) model, together with the solar EUV flux measured by the Solar Dynamics Observatory (SDO) EUV Variability Experiment (EVE). The study was conducted with data observed over European, Australian and South African stations from 2011 to 2013. Our results show differences in the TEC response to solar EUV over southern and Northern Hemispheric stations. The modeled TEC is consistent with the observed TEC over South African station, while it shows an underestimation with respect to the observed TEC over European stations.

The ionospheric delay estimated with the modeled TEC agrees with the delay estimated for observed TEC. The mean delay for the observed TEC is about 17.3 hours, while it is 16.4 hours for the modeled TEC. The mean correlation with the solar flux measured by SDO EVE is always higher in the case of the model-simulated TEC than for the observed TEC.

Zusammenfassung: Wir untersuchen die ionosphärische Reaktion auf solare extreme ultraviolette (EUV) Schwankungen unter Verwendung des ionosphärischen Gesamtelektronengehalts (TEC) des International GNSS Service (IGS) und simuliert vom CTIPe-Modell (Coupled Thermosphere Ionosphere Plasmasphere Electrodynamics) gegen den vom Solar Dynamics Observatory (SDO) EVE gemessenen solaren EUV-Fluss. Die Studie verwendet Daten aus den Jahren 2011 bis 2013 an europäischen, australischen und südafrikanischen Stationen. Unsere Ergebnisse zeigen eine unterschiedliche TEC-Reaktion über Stationen der südlichen und nördlichen Hemisphäre. Der modellierte TEC stimmt mit dem beobachteten TEC über südafrikanischen Stationen überein, während er eine Unterschätzung in Bezug auf den beobachteten TEC über europäischen Stationen zeigt.

Darüber hinaus stimmt die unter Verwendung von modellsimuliertem TEC geschätzte ionosphärische Verzögerung mit dejenigen für beobachteten TEC überein. Eine durchschnittliche Verzögerung für den beobachteten TEC beträgt etwa 17,3 Stunden, während der modellierte TEC 16,4 Stunden beträgt. Darüber hinaus ist die mittlere Korrelation mit EUV-Beobachtungen bei modelliertem TEC stärker als bei beobachtetem TEC.

1 Introduction

The Sun emits electromagnetic radiation in a wide spectral range, including ultraviolet/extreme ultraviolet (UV/EUV) radiation, which affects the thermosphere-ionosphere (T-I) system as these spectral ranges are absorbed in the T-I, leading to ionization and thus, the formation of the ionosphere. UV and EUV radiation varies on different time scales, including the prevailing 11-year cycle and, on shorter time scales, the 27-day solar rotation period. The EUV/UV radiation is responsible for the ionization and photodissociation of major neutrals, in particular atomic oxygen, molecular nitrogen, and molecular oxygen, and in this way contributes to the vertical and horizontal distribution of electron density. Solar EUV radiation has only been observed continuously since the launch of the TIMED / SEE mission in 2002 (Woods et al., 2000; Woods, 2005), see also the review by Schmidtke (2015). Therefore, it is often represented by solar proxies, the most prominent one being the F10.7 index (Tapping, 2013).

The influence of solar radiation on the T-I system has been extensively studied by many researchers (e.g. Kutiev et al., 2013; Jacobi et al., 2016; Vaishnav et al., 2018, 2019a). The state of the ionosphere is characterized by different parameters, including the total electron content (TEC, given in units of 1 TECU = 10^{16} electrons m^{-2}), i.e., the vertically integrated electron density. Otherwise, used parameters are the peak electron density (NmF2, cm^{-3}) and the corresponding height (hmF2, km). Unglaub et al. (2011, 2012) used the EUV-TEC proxy from combined EUV spectra observed by TIMED-SEE and SDO-EVE to study the ionospheric response. Solar activity plays a significant role in the ionospheric effect on solar variability (Vaishnav et al., 2021a). Vaishnav et al. (2019b) suggested that during solar cycle (SC) 23, the correlation between solar proxies and ionospheric TEC was stronger than during SC 24. This is likely due to the longer lifetime of active regions during SC 23. The wavelet variance estimation method suggests that the variance is more significant during SC 23 than during SC 24.

Several authors have reported an ionospheric delay of about one day with respect to solar EUV radiation or solar proxies on the time scale of the 27-day solar rotation period (e.g. Jakowski et al., 1991; Min et al., 2009; Jacobi et al., 2016; Schmölter et al., 2018; Vaishnav et al., 2018, 2019a). In recent years, the delay has been more accurately estimated due to the availability of high-resolution EUV measurements and has been reported to be about 17 hours, modified by latitude and season (Schmölter et al., 2018; Schmölter et al., 2020; Vaishnav et al., 2021b). Initial attempts to model the delay were made by Jakowski et al. (1991), who used a one-dimensional numerical model between 100 and 250 km altitude with simplifying assumptions to investigate the physical mechanism of ionospheric delay. They proposed that a delay of about 2 days in atomic oxygen at 180 km altitude occurs due to photodissociation of molecular oxygen and transport processes.

Preliminary investigation by Vaishnav et al. (2018) also showed the possible role of transport processes in ionospheric delay using the Coupled Thermosphere Ionosphere Plasmasphere Electrodynamics (CTIPe, Fuller-Rowell and Rees (1983); Codrescu et al. (2012)) model simulations. In addition, Ren et al. (2018) suggested a possible contribution of photochemical and electrodynamic processes in the ionospheric delayed response using the Thermosphere Ionosphere Electrodynamics-General Circulation Model (TIE -GCM) simulations. The delay is due to the different response times between the quasi-

instantaneous ionization and the slower recombination in the ionospheric F region.

Vaishnav et al. (2021b) investigated the ionospheric delay and showed good agreement between the estimated delay between the model-simulated TEC and the observed TEC with the flux measured by Solar Dynamics Observatory (SDO) in the extreme ultraviolet (EUV) Variability Experiment (EVE). The average delay for the observed (modeled) TEC is 17(16) hours. The average delay calculated for the observed and modeled TEC is 1 and 2 hours longer, respectively, for the Southern Hemisphere than for the Northern Hemisphere. Schmölter et al. (2020) also showed the latitudinal and seasonal variations in the ionospheric delay and also discussed the possible role of geomagnetic activity. In addition, Vaishnav et al. (2021a) discussed the possible contribution and role of eddy diffusion in the delayed ionospheric response. They showed that eddy diffusion is one of the important sources directly affecting the ionospheric delay. Increasing eddy diffusion leads to a decrease in ionospheric delay.

The present study aims to analyse the TEC variations of the ionosphere in the Northern and Southern Hemispheres during moderate solar activity phases in SC 24, 2011 to 2013. This analysis uses GNSS data over European, Australian and South African stations. The observed TEC properties are compared with the model-simulated TEC. In Section 2, we present our data sources and the CTIPe model used for the analyses. In Section 3, we investigate the variability of TEC, a possible relationship with the F10.7 index, and the periodicity estimation. In Section 4, we summarize our conclusions.

2 Data sources and numerical model used

2.1 TEC observations

In this paper, we use TEC, extracted from the International GNSS Service (IGS) TEC maps provided by NASA's CDDIS (Noll, 2010), which have a time resolution of 1 hour and a latitude and longitude resolution of $2.5^\circ \times 5^\circ$ (Hernández-Pajares et al., 2009). The GNSS data collected were used from grid points near different stations in the Northern and Southern Hemispheres. The stations used from Europe are Arnstein and Rome in the Northern Hemisphere. For the Southern Hemisphere region, Bloemfontein in South Africa and Canberra in Australia were selected. We used the nearest grid points in TEC maps available near the ground stations, weighted more by observations and less by the model used in TEC map generation to fill temporal and spatial gaps.

Figure 1 shows a map depicting the study sites used to calculate the ionospheric delay in the Northern and Southern Hemispheres.

2.2 Solar EUV radiation

To investigate the influence of solar EUV radiation on the variability of the ionosphere, both solar EUV flux observations and solar proxies are often used. The SDO-EVE instrument provides a continuous high-resolution spectra with a wavelength range of 0.1 to 120 nm, a spectral resolution of 0.1 nm, and a temporal resolution of 20s (Woods et al., 2010; Pesnell et al., 2011). The high-resolution observations provided by SDO were used here on an hourly basis to calculate an ionospheric delay in TEC.

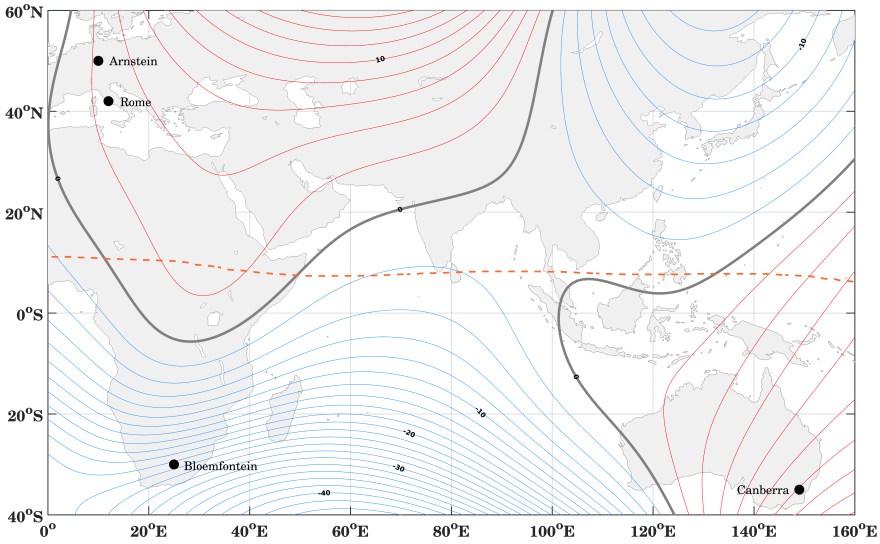

Figure 1: *Map depicting the study locations: European (Arnstein and Rome), South African (Bloemfontein) and Australian (Canberra) GPS stations. The Earth's magnetic field is shown by the geomagnetic equator (orange dashed line) and magnetic declination (blue, red, and black lines). The magnetic field data were taken from the World Magnetic Model (NASA, 2014).*

2.3 CTIPe Model

The CTIPe model is a global, three-dimensional, numerical, physics-based coupled thermosphere-ionosphere-plasmasphere model that self-consistently solves the primitive continuity, momentum, and energy equations to calculate the wind components, global temperature, and neutral composition, and is further used to calculate plasma production, loss, and transport. The model consists of four components, namely (a) a neutral thermosphere model (Fuller-Rowell and Rees, 1980), (b) a convection model for the mid- and high-latitude ionosphere (Quegan et al., 1982), (c) a plasmasphere and low-latitude ionosphere model (Millward et al., 1996), and (d) an electrodynamic model (Richmond et al., 1992). The calculations are performed at a resolution of 2°/18° in latitude/longitude. In the vertical direction, the atmosphere is divided into 15 logarithmic pressure levels at intervals of one scale height, starting with a lower boundary at 1 Pa (about 80 km altitude) to over 500 km altitude at pressure level 15. External inputs are required to run the model, such as solar UV and EUV radiation, the Weimer electric field, TIROS /NOAA Aurora precipitation, and tidal forcing from the Whole Atmosphere Model (WAM). The F10.7 index is used as a solar proxy to calculate ionization, heating, and oxygen dissociation processes in the ionosphere. Detailed information on CTIPe can be found in Codrescu et al. (2008, 2012).

3 Results

3.1 TEC variations at moderate solar activity of solar cycle 24

The behavior of the T-I system varies greatly depending on the conditions of solar activity. Figure 2 shows the averaged midday (11:00-13:00 LT) variations in TEC from 2011

Table 1: *Geographic latitudes and longitudes of European (Arnstein and Rome), South African (Bloemfontein), and Australian (Canberra) GPS stations and the nearest CTIPe model grid points used to investigate the TEC variations delayed ionospheric response.*

Station	Geog. Lat (°)	Geog. Long (°)	CTIPe Geog. Lat (°)	CTIPe Geog. Lon (°)
Arnstein	50	10	50	18
Rome	41.8	12.5	42	18
Bloemfontein	-30	25	-30	18
Canberra	-35.3	149	-36	144

to 2013 during SC 24. The figure shows the comparison between the observed TEC (red) and the modeled TEC (blue) simulated with the EUVAC flux model for Arnstein, Rome, Canberra and Bloemfontein. The integrated SDO EVE flux (1-120 nm) is shown on the second y-axis of figure 2a.

The variation of the TEC level during the different seasons and the varying solar activity can be seen in the time series. The ionospheric electron density distribution is mainly controlled by photoionization, dissociation, and transport processes, as well as loss through recombination processes. Variations in the observed TEC vary with location, such as Southern Hemisphere and Northern Hemisphere.

Figures 2(a) show that there are continuously pronounced 27-day cycles in the SDO EVE flux in 2012. This type of regular variation in the solar observations provides us an opportunity to study the corresponding ionospheric variations. The observed TEC variations over the Arnstein site are larger during the spring season and smaller during the winter season. Compared to the observed TEC, the modeled TEC is underestimated during the spring and summer periods, while it is in good agreement during the winter season. The overall level of TEC is lower compared to the other study stations. The discrepancy between the modeled and observed TEC is higher during the spring and summer seasons. Above this site, the modeled TEC mostly underestimates the observed TEC.

Compared to the TEC level at Arnstein, TEC shows opposite characteristics at Rome (Figure 2(b)). Above this site, the modeled TEC overestimates the observed TEC during the winter months, while it shows underestimation during the summer months. The observed TEC in Arnstein and Rome is comparable, but the modeled TEC is higher in Rome. This is due to the fact that maximum ionization occurs at the equator and in low latitude regions. The TEC value decreases towards high latitudes. Therefore, the TEC values are higher in Rome than in Arnstein.

Figure 2(c) shows the TEC level during 2011-2013 over the Australian station Canberra. Here, the maximum of TEC is observed during March-April (autumn) and November (spring) in 2011. Over this site, the modeled TEC is in good agreement with the observed TEC during the spring months. During the autumn and winter months, the observed TEC is underestimated by the modeled TEC.

Figure 2(d) shows the variations over the South African station Bloemfontein. The modeled TEC shows an overestimation compared to the observed TEC during the spring

season. Except during the spring months, the modeled TEC level is in good agreement with the observed TEC level during midday over Bloemfontein. It can be seen that the TEC levels are almost the same depending on the moderate solar activity conditions during the study period.

In general, TEC levels vary latitudinally and longitudinally depending on the time of year both in the Northern and at Southern Hemisphere. The TEC simulated by the CTIPe model agrees better with the Southern Hemispheric stations than with the Northern Hemispheric stations. The spatial distribution of TEC depends on the ionization of neutrals, transport processes, and recombination, which varies with latitude and longitude. The variations in TEC are not only controlled by solar irradiance, but there are other factors such as local dynamics, or geomagnetic activities due to solar wind variations that also affect the ionospheric state (Abdu, 2016).

The TEC values over Southern Hemispheric stations are higher than the Northern Hemispheric values and the TEC values change faster from the southern to the Northern Hemisphere values, causing the annual anomaly (Romero-Hernandez et al., 2018).

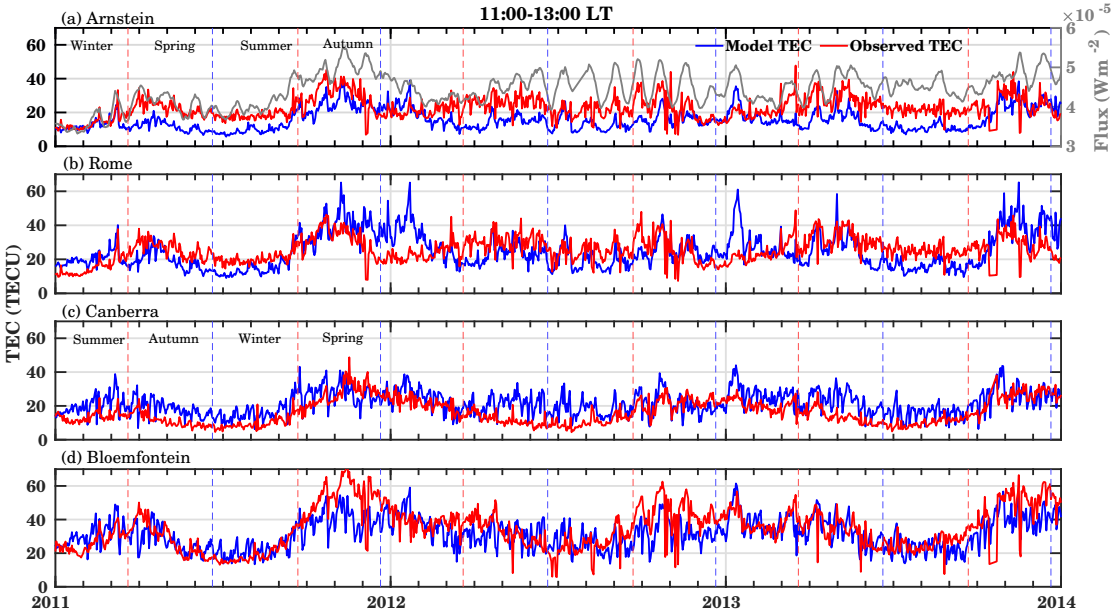

Figure 2: *Comparison between observed TEC and model-simulated TEC at midday (11:00-13:00 LT) for different locations: (a) Arnstein, (b) Rome, (c) Canberra, and (d) Bloemfontein. The gray curve in panel (a) represents the integrated SDO EVE flux (1-120 nm).*

3.2 Periodicity estimation

To investigate the oscillatory behavior in the time series of TEC across all stations, the continuous wavelet transfer method (CWT) was used. The CWT captures the impulsive events at the same times they occur in the time series (Percival and Walden, 2000). However, the CWT also examines the low-frequency features of the data that are hidden in the time series. Several authors have reported the oscillatory behavior of solar and ionospheric parameters using the wavelet method (e.g. Vaishnav et al., 2018). The solar activity varies on different time scales from minutes to 11-year solar cycle and beyond.

Recently, Vaishnav et al. (2021b) used the CWT technique to study the periodicity during 2011 to 2013 for low, mid, and high latitudes. Here, we use a similar technique to examine the dominant periods over our study locations, as shown in Table 1. The uninterpreted data of daily observed and modeled TEC during 2011 to 2013 are used to analyze the periodic behavior of the T-I system.

Here we will examine and compare the different temporal patterns of observed and modeled global TEC. Figure 3 shows the continuous wavelet spectra of the model-simulated and observed TEC for different stations from 2011 to 2013. The white line represents the corresponding time series used to calculate the CWT.

The top panel (a-c) and bottom panel (d-f) of Figure 3 show the CWT of modeled TEC and observed TEC, respectively, over three different sites, as mentioned in the figure title. The most dominant period observed in the modeled TEC is 16-32 days in 2012 across all stations. During this study period, 16-32 day periodicity has been observed in the F10.7 index, e.g., by Vaishnav et al. (2021b). This dominant period is weaker in 2011 and 2013. During this period, the influence of other dynamical processes in the ionosphere (e.g., lower atmospheric forcing) is stronger. A very weak 27-day periodicity was observed in these years. The 27-day periodicity is stronger in the winter season. Pancheva et al. (1991) suggested a possible cause for the 27-day variation in the lower ionosphere (D region), which is often caused by dynamical forcing, especially in the winter season under conditions of low solar activity.

Especially over Bloemfontein and Canberra there is a dominance of the period range of 8-16 days. In addition, another strong region is visible in the 128-256 day period range, representing the semi-annual oscillations in both the modeled and observed TEC. The semi-annual oscillation is most dominant during our study period. Compared to the modeled TEC, the 27-day periodicity is weaker in the observed TEC, as shown in Figure 3(d-f). The dominant period is observed only during the September-October months of each year. The 64-128-day periodicity is not observed in the observations, but is seen in the modeled TEC.

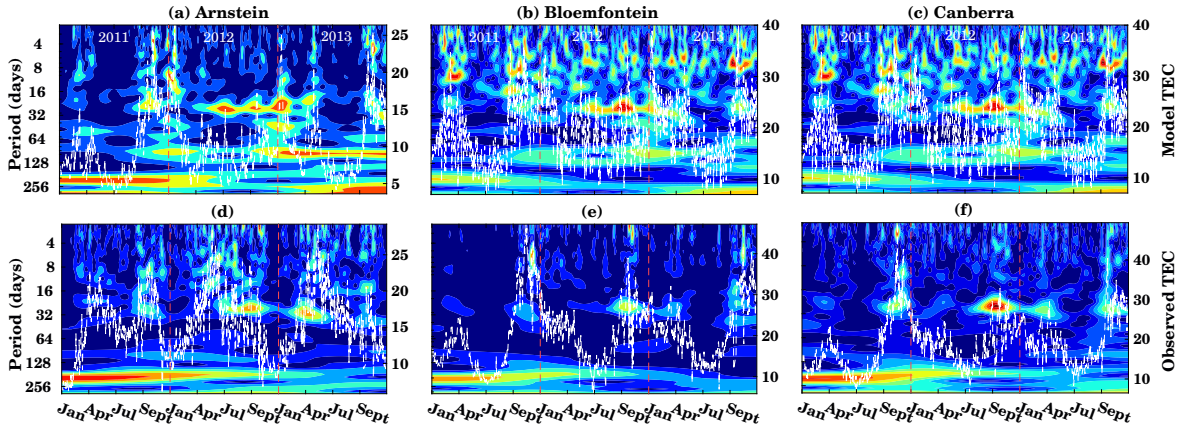

Figure 3: *Continuous wavelet spectra of modeled TEC (a-c) and observed TEC (d-f) for Arnstein, Bloemfontein and Canberra. The white lines show the corresponding time series.*

3.3 Cross-correlation and delay estimation

The delayed response of the ionosphere to solar EUV observations and solar proxies has been studied by several authors and they reported an ionospheric delay of about 1-2 days (Jakowski et al., 1991; Jacobi et al., 2016; Vaishnav et al., 2019a). Using the high-resolution SDO EVE and GOES EUV fluxes against TEC, a more accurate ionospheric delay of about 17 hours was reported (Schmölter et al., 2020). The observed delay is also confirmed by numerical physics-based models (Ren et al., 2018; Vaishnav et al., 2018, 2021b).

Figure 4 shows the cross-correlation and a corresponding ionospheric delay calculated using observed and modeled TEC with the integrated SDO EVE flux in the wavelength range from 1 to 120 nm over the study sites listed in Table 1. The modeled TEC, used for these analyses, was simulated using the EUVAC solar flux model within CTIPe and the F10.7 index as a solar proxy to calculate the input spectra. Here, the cross-correlation and lag are calculated for each month from 2011 to 2013.

The results over the Northern Hemispheric stations are shown in Figure 4 (a-b). The upper panel shows the correlation coefficient, and the corresponding lower panel shows the ionospheric delay. The trend for the correlation coefficient over both European sites calculated for observed TEC is similar, which is also true for the ionospheric lag. This is consistent with similar results from Schmölter et al. (2020).

We compare the correlation coefficient and ionospheric delay calculated with the observed TEC with the simulated model TEC. The correlation coefficients generally agree over Arnstein and are only slightly higher than the observed values. Similar variations are seen over Rome. The bottom panel of the figure 4 (a-b) shows the corresponding ionospheric delay. Here, the ionospheric delay from the observations at both locations is almost similar, and the average ionospheric delay during this study period is about 15-19 hours. The minimum delay from the observations is about 6 hours in August 2012 TEC, while from the model simulation TEC it has a delay of 22 hours. In general, the ionospheric delay calculated from the modeled TEC is in good agreement over the European sites. Of particular note is the annual decrease in delay during the winter season reported by Schmölter et al. (2020), which is well reproduced by the model.

Figure 4(c) shows the correlation coefficient and ionospheric delay over the Australian station Canberra. Here the model correlation coefficient is generally slightly higher than the observed one. The lower panel shows the ionospheric delay. The ionospheric delay calculated from the model simulation TEC agrees with the observed one, but the difference is slightly larger in 2011, and amounts to about 5 hours. The seasonal characteristics show the same tendency as those of the stations from Northern Hemisphere, but the scatter is larger.

A similar characteristic is observed at the South African station (Figure 4(d)). The ionospheric delay in the model-simulated TEC is very small, about 5 hours for November 2012.

An average ionospheric delay for the observed TEC is about 17.3 hours and 16.4 hours for the modeled TEC across all stations. An average difference between the Northern and Southern Hemispheric stations is about 1 hour for the observed TEC, while it is 2 hours for the modeled TEC. Our analysis shows that the ionospheric delay is longer in the case of the observed Southern Hemisphere than in the case of the modeled TEC,

while the model shows an opposite characteristic with a difference of about 2 hours. Moreover, the cross-correlation analysis shows that the mean correlation in the case of the modeled TEC is about 0.2, while it is 0.1 in the case of the observed TEC against the solar flux measured by SDO EVE. This indicates that in the real observations the ionospheric behavior is not only controlled by the solar activity, but also other factors, e.g. meteorological influences, play a significant role. During some months even a negative correlation was observed both in the model and in the observations. This negative correlation indicates the influence of local dynamics. The correlation coefficients at the Southern Hemispheric stations are generally higher than at the Northern Hemispheric stations.

In general, the ionospheric delay seen in the observed TEC is successfully reproduced by the CTIPe model simulated TEC and is about 17 hours. The seasonal variability of the delay is also captured by the model. Vaishnav et al. (2021b) examined the delayed ionospheric response at 15°E and found that the average delay calculated for observed and modeled TEC is 1 and 2 hours longer for Southern Hemisphere than for Northern Hemisphere. The ionospheric delay is related to the change in the ratio of atomic oxygen to molecular nitrogen, as suggested by Ren et al. (2018).

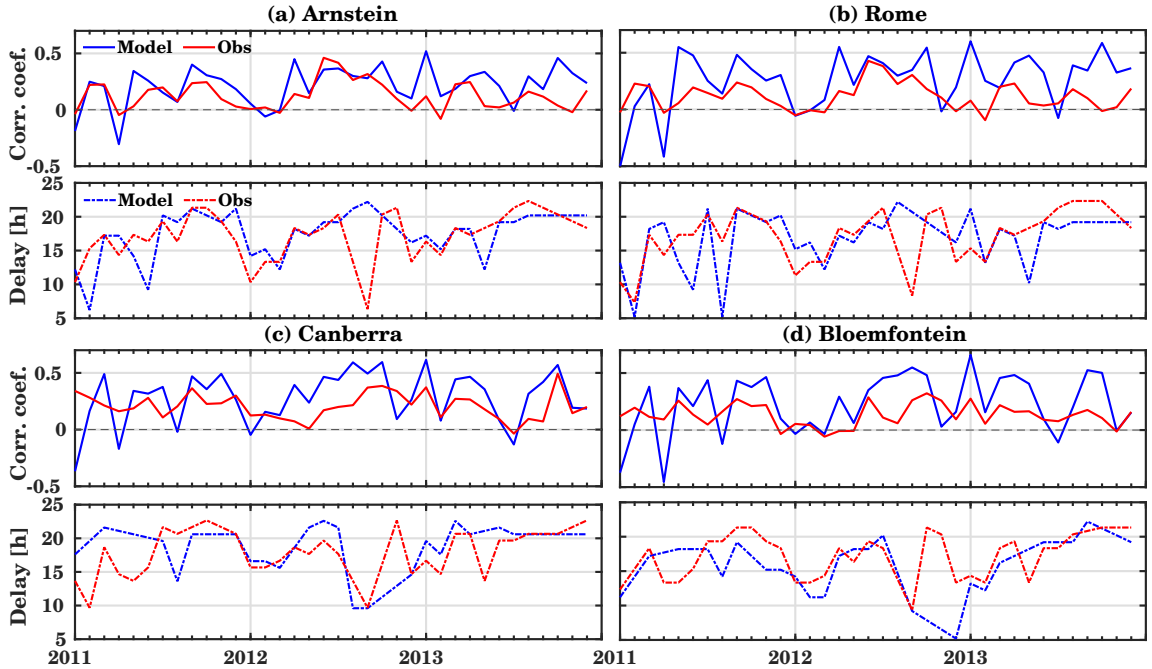

Figure 4: *Time series of correlation coefficients and delay estimations for different locations (a) Arnstein, (b) Rome, (c) Canberra and (d) Bloemfontein using observed and model simulated TEC with solar EUV flux from SDO EVE.*

4 Conclusions

We analyzed the ionospheric TEC from TEC maps provided by the International GNSS Service (IGS) and simulated it with the CTIPe model against the solar EUV flux measured by the SDO EVE satellite and its trend during 2011-2013 over European, Australian and South African stations. The modeled TEC is in agreement with the observed

TEC over South African, while it shows an underestimation with respect to the observed TEC over European stations.

In addition, the ionospheric delay estimated with the model TEC agrees with the delay estimated for observed TEC. The mean delay for the observed TEC is about 17.3 hours, while it is 16.4 hours for the modeled TEC. Moreover, the mean correlation with the solar flux measured by SDO EVE is always higher in the case of modeled TEC than observed TEC.

Acknowledgements IGS TEC maps have been kindly provided via NASA through ftp://cddis.gsfc.nasa.gov/gnss/products/ionex/. SDO-EVE data have been provided by the Laboratory for Atmospheric and Space Physics (LASP) through http://lasp.colorado.edu/eve/data_access/evewebdata (LASP, 2018a). Daily F10.7 index can be downloaded from http://lasp.colorado.edu/lisird/data/noaa_radio_flux/ (LASP, 2018b). The study has been supported by Deutsche Forschungsgemeinschaft (DFG) through grants nos. JA 836/33-1 and BE 5789/2-1.

References

Abdu, M. A.: Electrodynamics of ionospheric weather over low latitudes, Geoscience Letters, 3, doi:10.1186/s40562-016-0043-6, 2016.

Codrescu, M. V., Fuller-Rowell, T. J., Munteanu, V., Minter, C. F., and Millward, G. H.: Validation of the Coupled Thermosphere Ionosphere Plasmasphere Electrodynamics model: CTIPE-Mass Spectrometer Incoherent Scatter temperature comparison, Space Weather, 6, doi:10.1029/2007sw000364, 2008.

Codrescu, M. V., Negrea, C., Fedrizzi, M., et al.: A real-time run of the Coupled Thermosphere Ionosphere Plasmasphere Electrodynamics (CTIPe) model, Space Weather, 10, doi:10.1029/2011sw000736, 2012.

Fuller-Rowell, T. and Rees, D.: Derivation of a conservation equation for mean molecular weight for a two-constituent gas within a three-dimensional, time-dependent model of the thermosphere, Planetary and Space Science, 31, 1209–1222, doi:10.1016/0032-0633(83)90112-5, 1983.

Fuller-Rowell, T. J. and Rees, D.: A Three-Dimensional Time-Dependent Global Model of the Thermosphere, Journal of the Atmospheric Sciences, 37, 2545–2567, doi:10.1175/1520-0469(1980)037<2545:atdtdg>2.0.co;2, 1980.

Hernández-Pajares, M., Juan, J. M., Sanz, J., et al.: The IGS VTEC maps: a reliable source of ionospheric information since 1998, Journal of Geodesy, 83, 263–275, doi:10.1007/s00190-008-0266-1, 2009.

Jacobi, C., Jakowski, N., Schmidtke, G., and Woods, T. N.: Delayed response of the global total electron content to solar EUV variations, Advances in Radio Science, 14, 175–180, doi:10.5194/ars-14-175-2016, 2016.

Jakowski, N., Fichtelmann, B., and Jungstand, A.: Solar activity control of ionospheric and thermospheric processes, Journal of Atmospheric and Terrestrial Physics, 53, 1125–1130, doi:10.1016/0021-9169(91)90061-B, 1991.

Kutiev, I., Tsagouri, I., Perrone, L., et al.: Solar activity impact on the Earth's upper atmosphere, Journal of Space Weather and Space Climate, 3, A06, doi:10.1051/swsc/2013028, 2013.

LASP: EVE Data, available at: `http://lasp.colorado.edu/eve/data_access/evewebdata`, last access: 15 August 2018, 2018a.

LASP: F10.7 index, available at: `http://lasp.colorado.edu/lisird/data/noaa_radio_flux/`, last access: 15 August 2018, 2018b.

Millward, G., Moffett, R., Quegan, S., and Fuller-Rowell, T.: A coupled thermosphere-ionosphere-plasmasphere model (CTIP), STEP handbook on ionospheric models, pp. 239–279, 1996.

Min, K., Park, J., Kim, H., et al.: The 27-day modulation of the low-latitude ionosphere during a solar maximum, Journal of Geophysical Research: Space Physics, 114, 1–8, doi:10.1029/2008JA013881, 2009.

NASA: Shapefiles for declination and inclination of the World Magnetic Model, available at: ftp://ftp.ngdc.noaa.gov/geomag/wmm/wmm2015/shapefiles/2015/, last access: 15 August 2018, 2014.

Noll, C. E.: The crustal dynamics data information system: A resource to support scientific analysis using space geodesy, Advances in Space Research, 45, 1421–1440, doi:10.1016/j.asr.2010.01.018, 2010.

Pancheva, D., Schminder, R., and Laštovička, J.: 27-day fluctuations in the ionospheric D-region, Journal of Atmospheric and Terrestrial Physics, 53, 1145–1150, doi:10.1016/0021-9169(91)90064-e, 1991.

Percival, D. B. and Walden, A. T.: Wavelet Methods for Time SeriesAnalysis, Cambridge University Press, doi:10.1017/cbo9780511841040, 2000.

Pesnell, W. D., Thompson, B. J., and Chamberlin, P. C.: The Solar Dynamics Observatory (SDO), Solar Physics, 275, 3–15, doi:10.1007/s11207-011-9841-3, 2011.

Quegan, S., Bailey, G. J., Moffett, R. J., et al.: A theoretical study of the distribution of ionization in the high-latitude ionosphere and the plasmasphere: first results on the mid-latitude trough and the light-ion trough, Journal of Atmospheric and Terrestrial Physics, 44, 619–640, doi:10.1016/0021-9169(82)90073-3, 1982.

Ren, D., Lei, J., Wang, W., et al.: Does the Peak Response of the Ionospheric F2 Region Plasma Lag the Peak of 27-Day Solar Flux Variation by Multiple Days?, Journal of Geophysical Research: Space Physics, pp. 1–11, doi:10.1029/2018JA025835, 2018.

Richmond, A. D., Ridley, E. C., and Roble, R. G.: A thermosphere/ionosphere general circulation model with coupled electrodynamics, Geophysical Research Letters, 19, 601–604, doi:10.1029/92GL00401, 1992.

Romero-Hernandez, E., Denardini, C. M., Takahashi, H., et al.: Daytime ionospheric TEC weather study over Latin America, Journal of Geophysical Research: Space Physics, doi:10.1029/2018ja025943, 2018.

Schmidtke, G.: Extreme ultraviolet spectral irradiance measurements since 1946, History of Geo- and Space Sciences, 6, 3–22, doi:10.5194/hgss-6-3-2015, 2015.

Schmölter, E., Berdermann, J., Jakowski, N., Jacobi, C., and Vaishnav, R.: Delayed response of the ionosphere to solar EUV variability, Advances in Radio Science, 16, 149–155, doi:10.5194/ars-16-149-2018, 2018.

Schmölter, E., Berdermann, J., Jakowski, N., and Jacobi, C.: Spatial and seasonal effects on the delayed ionospheric response to solar EUV changes, Annales Geophysicae, 38, 149–162, doi:10.5194/angeo-38-149-2020, 2020.

Tapping, K. F.: The 10.7 cm solar radio flux (F10.7), Space Weather, 11, 394–406, doi:10.1002/swe.20064, 2013.

Unglaub, C., Jacobi, C., Schmidtke, G., Nikutowski, B., and Brunner, R.: EUV-TEC proxy to describe ionospheric variability using satellite-borne solar EUV measurements: First results, Advances in Space Research, 47, 1578–1584, doi:10.1016/j.asr.2010.12.014, 2011.

Unglaub, C., Jacobi, C., Schmidtke, G., Nikutowski, B., and Brunner, R.: EUV-TEC proxy to describe ionospheric variability using satellite-borne solar EUV measurements, Advances in Radio Science, 10, 259–263, doi:10.5194/ars-10-259-2012, 2012.

Vaishnav, R., Jacobi, C., Berdermann, J., Schmölter, E., and Codrescu, M.: Ionospheric response to solar EUV variations: Preliminary results, Advances in Radio Science, 16, 157–165, doi:10.5194/ars-16-157-2018, 2018.

Vaishnav, R., Jacobi, C., and Berdermann, J.: Long-term trends in the ionospheric response to solar extreme-ultraviolet variations, Annales Geophysicae, 37, 1141–1159, doi:10.5194/angeo-37-1141-2019, 2019a.

Vaishnav, R., Jacobi, C., Berdermann, J., Codrescu, M., and Schmölter, E.: Ionospheric response to solar variability during solar cycles 23 and 24, Rep. Inst. Meteorol. Univ. Leipzig, 57, 97–106, URL https://nbn-resolving.org/urn:nbn:de:bsz:15-qucosa2-741822, 2019b.

Vaishnav, R., Jacobi, C., Berdermann, J., Codrescu, M., and Schmölter, E.: Role of eddy diffusion in the delayed ionospheric response to solar flux changes, Annales Geophysicae, 39, 641–655, doi:10.5194/angeo-39-641-2021, 2021a.

Vaishnav, R., Schmölter, E., Jacobi, C., Berdermann, J., and Codrescu, M.: Ionospheric response to solar

extreme ultraviolet radiation variations: comparison based on CTIPe model simulations and satellite measurements, Annales Geophysicae, 39, 341–355, doi:10.5194/angeo-39-341-2021, 2021b.

Woods, T., Bailey, S., Eparvier, F., et al.: TIMED Solar EUV experiment, Physics and Chemistry of the Earth, Part C: Solar, Terrestrial & Planetary Science, 25, 393–396, doi:10.1016/s1464-1917(00)00040-4, 2000.

Woods, T. N.: Solar EUV Experiment (SEE): Mission overview and first results, Journal of Geophysical Research, 110, doi:10.1029/2004ja010765, 2005.

Woods, T. N., Eparvier, F. G., Hock, R., et al.: Extreme Ultraviolet Variability Experiment (EVE) on the Solar Dynamics Observatory (SDO): Overview of Science Objectives, Instrument Design, Data Products, and Model Developments, Solar Physics, 275, 115–143, doi:10.1007/s11207-009-9487-6, 2010.